Stability analysis of predictor-corrector schemes for coupling neutronics and depletion

P. Cosgrove, E. Shwageraus, G.T. Parks

Department of Engineering, University of Cambridge, Trumpington Street, Cambridge, CB2 1PZ, United Kingdom

Abstract

Numerical instability resulting from coupling isotopic depletion and neutronics is widely reported, but little work has been done to interrogate the phenomenon theoretically. This work extends the pioneering analysis developed by Densmore et al., who examined the stability of a monoenergetic neutron diffusion problem coupled with a simple depletion system through the explicit Euler scheme. Their Fourier stability analysis is applied to the predictor-corrector scheme and its iterated and implicit variants. The results reproduce behaviour described in previous reports of numerical instability and its solution, and develop a future avenue for diagnosing the stability of burn-up problems.

Keywords: Depletion, Neutron transport, Monte Carlo, Stability

1. Introduction

Nuclear reactor analysis inevitably requires burn-up calculations to determine how the reactor criticality, power profile, and isotopic field vary during operation. Burn-up calculations refer to the simultaneous solution of the neutron transport or diffusion equation and the Bateman equation – a coupled, non-linear system ensues. Typically, burn-up problems are solved using a quasi-static approximation, neglecting the dynamics of the transport or diffusion equation, and instead coupling their eigenvalue form to the Bateman equation.

The numerical solution of this system is subject to the common concerns of accuracy and stability. Accuracy is the more prominent and has been subject to more substantial analysis in recent research, resulting in the development of several neutronics-depletion coupling schemes (Isotalo and Aarnio, 2011a,b; Isotalo and Sahlberg, 2015; Josey, 2017). However, the stability of these scheme has also received some consideration, particularly in spatially large systems where a Monte Carlo solution is used for neutronics. The stochastic characteristics of the Monte Carlo solution have been shown to affect numerical stability, but are not solely responsible for it (Cosgrove et al., 2020b). The most thorough stability analysis of a neutronics-depletion system to date was performed by Densmore et al. (2013),

Email address: pmc55@cam.ac.uk (P. Cosgrove)

showing that instability can arise in deterministic systems and is affected by time-step length. Furthermore, although enforcing xenon equilibrium is often sufficient to prevent non-physical behaviour in common reactor problems (Griesheimer, 2010; Isotalo et al., 2013), there was no explicit xenon analogue in the system considered by Densmore et al., highlighting that enforcing xenon equilibrium does not necessarily result in an unconditionally stable system.

The analysis performed by Densmore et al. was applied to the mono-energetic diffusion equation coupled to depletion using the explicit Euler method. The explicit Euler method is ubiquitous, although relatively rarely used in production calculations due to its low-order accuracy in time – several other methods are more commonly applied, both for improved accuracy and stability.

This work extends the analysis of Densmore et al. to several more complicated coupling schemes. This will begin with a refresher on several neutronics depletion schemes. Following this, the neutronics-depletion systems to be examined are formulated and subjected to a Fourier/Von Neumann stability analysis – the initial portion of this examination is necessarily a repetition of that given by Densmore et al., and so it will be highlighted explicitly where any differences occur and where the original portion of the analysis begins.

2. Neutronics-depletion schemes

Many different neutronics-depletion coupling schemes exist, most of them focused on improved accuracy and some on improved stability. Those to be examined are described in this section.

The Bateman equation is given by (Bell and Glasstone, 1970):

$$\frac{\partial N}{\partial t} = \mathbf{A}N \tag{1}$$

Here N is the nuclide density vector at a point or in an infinite homogeneous medium, t is the time variable, and $\mathbf{A}$ is the burn-up matrix, describing the per-nuclide loss and gain rate due to fission, decay, and transmutation. Many codes numerically solve the discretised Bateman equation for a fixed burn-up matrix by using its formal matrix exponential solution:

$$N_{n+1} = \exp\left[\mathbf{A}\Delta t\right] N_n \tag{2}$$

Here N_n is the initial nuclide density (at time-point n), N_{n+1} is the 'burned' nuclide density obtained for the subsequent time-point, and Δt is the time-step length. This matrix exponential can be efficiently and accurately evaluated using the Chebyshev Rational Approximation Method (Pusa, 2013). Due to fission and transmutation, the burn-up matrix is a function of the flux, ϕ, to which the material region is subjected:

$$\mathbf{A} = \mathbf{A}(\phi) \tag{3}$$

This flux is obtained from a generic neutronics solver which takes the nuclide density field as an input. Therefore, burn-up is a non-linear problem.

The simplest approach to solving this coupled system is to fix the burn-up matrix at a given point in time; for some initial nuclide density field N_0 with a corresponding neutronics solution ϕ_0, the subsequent nuclide density field is simply:

$$N_1 = \exp[\mathbf{A}(\phi)\Delta t]N_0 \tag{4}$$

The explicit Euler scheme is shown in Algorithm 1. Note, as Isotalo highlights, this scheme is not a true explicit Euler scheme given that, due to the matrix exponential often applied, the time-derivative is not constant during the time-step (Isotalo, 2013). However, the explicit Euler scheme is not often applied in practice due to its low order, necessitating many brief time-steps to maintain accuracy.

Input: $N_0, n_{\text{steps}}, \Delta t$
for $n = 0, ..., n_{\text{steps}} - 1$ **do**
  $\mathbf{A}_n \leftarrow \phi(N_n)$
  $N_{n+1} \leftarrow \exp\left[\mathbf{A}_n \Delta t_n\right] N_n$
end

Algorithm 1: Explicit Euler method.

A common improvement is the predictor-corrector scheme, which is the basis for most other depletion schemes to follow. Here the constant extrapolation/linear interpolation (CE/LI) scheme described by Isotalo and Aarnio (2011a) is covered. The 'predictor' portion of this algorithm is identical to the explicit Euler scheme. However, the end-of-step (EOS) nuclide density field is used to obtain a corresponding EOS flux solution and burn-up matrix. By averaging this matrix alongside the beginning-of-step (BOS) matrix, a more representative time-averaged set of reaction rates can be obtained, increasing the accuracy at the cost of a second neutronics solution. This is shown in Algorithm 2.

Input: $N_0, n_{\text{steps}}, \Delta t$
for $n = 0, ..., n_{\text{steps}} - 1$ **do**
  $\mathbf{A}_n \leftarrow \phi(N_n)$
  $N_{n+1} \leftarrow \exp\left[\mathbf{A}_n \Delta t_n\right] N_n$
  $\mathbf{A}_{n+1} \leftarrow \phi(N_{n+1})$
  $\mathbf{A} \leftarrow \frac{1}{2}\left(\mathbf{A}_n + \mathbf{A}_{n+1}\right)$
  $N_{n+1} \leftarrow \exp\left[\mathbf{A} \Delta t_n\right] N_n$
end

Algorithm 2: Predictor-corrector method.

In order to accurately handle burnable absorbers, however, the need to use short time-steps remains with the simple CE/LI predictor-corrector scheme. This motivated the development of higher-order 'substep' methods (Isotalo and Aarnio, 2011a,b). These methods work by dividing depletion time-steps of length Δt into smaller substeps where the weighting between the BOS and EOS burn-up matrices varies at each substep. The analysis of these schemes is left for future work.

Each of the predictor-corrector methods can be modified to produce an implicit equivalent. This entails iterating on the corrector step while applying an underrelaxation factor, $0 < \alpha < 1$. The first of these methods to be introduced was the 'stochastic implicit' scheme (Dufek et al., 2013; Kotlyar and Shwageraus, 2014, 2016; Josey, 2017; Valtavirta and Leppänen, 2018), derived from the stochastic approximation (Robbins and Monro, 1951), where the relaxation factor varies with the number of corrector iterations as:

$$\alpha_j = \frac{1}{j+1} \tag{5}$$

Here j is the iteration number, beginning with $j = 0$. Although this method is relatively common, a fixed relaxation factor can also be used successfully in implicit coupling schemes and appears to be advantageous for common problems in terms of efficiency and stability (Cosgrove et al., 2020a). An implicit version of the predictor-corrector algorithm is shown in Algorithm 3.

Input: $N_0, n_{\text{steps}}, \Delta t, J, \alpha_j$
for $n = 0, ..., n_{\text{steps}} - 1$ **do**
  $\mathbf{A}_n \leftarrow \phi(N_n)$
  $N_{n+1}^{(0)} \leftarrow \exp\left[\mathbf{A}_n \Delta t_n\right] N_n$
  for $j = 0, ..., J - 1$ **do**
    $\mathbf{A}_{n+1} \leftarrow \phi(N_{n+1}^{(j)})$
    $\mathbf{A} \leftarrow \frac{1}{2}\left(\mathbf{A}_n + \mathbf{A}_{n+1}\right)$
    $N_{n+1}^{(j+1)} \leftarrow \alpha_j \exp\left[\mathbf{A} \Delta t_n\right] N_n + (1 - \alpha_j) N_{n+1}^{(j)}$
  end
  $N_{n+1} \leftarrow N_{n+1}^{(J)}$
end

Algorithm 3: Implicit predictor-corrector method.

3. Analysis

Having defined the algorithms which will be analysed, this section will begin by describing and justifying the simplified neutronics-depletion system to be examined before giving the predictor-corrector discretisation of the system. Perturbations to the nuclide and flux fields are decomposed into the harmonics of a cosine series and equations are obtained to describe how each harmonic grows. The initial equations are then modified to describe a predictor-corrector scheme with an iterated corrector step, with and without a relaxation factor.

The result of the stability analysis is a set of matrices describing the various depletion schemes and how they affect the evolution of the different spatial harmonics of the problem. The eigenvalues of these matrices will determine whether each spatial harmonic will be amplified or depressed over a series of time-steps. In particular, the spectral radius – or the eigenvalue with the largest magnitude – will determine the linear stability of a given depletion scheme and spatial mode. If the spectral radius is greater than one for a given harmonic, that harmonic is unstable.

3.1. Governing equations

Here we consider the 1D mono-energetic neutron diffusion equation subject to isotropic scattering in eigenvalue form:

$$-\frac{1}{3\Sigma_{\mathrm{t}}}\frac{\partial^2\phi}{\partial x^2}+\Sigma_{\mathrm{a}}\phi=\frac{1}{k}\nu\Sigma_{\mathrm{f}}\phi \tag{6}$$

In this equation, ϕ is the scalar neutron flux, x is the spatial variable, Σ_{t} is the total macroscopic cross-section, Σ_{a} is the macroscopic absorption cross-section, Σ_{f} is the macroscopic fission cross-section, ν is the average number of neutrons produced by fission, and k is the criticality eigenvalue. This is justified as problems in which burn-up instabilities have been reported tend to be large thermal problems where the diffusion approximation is reasonably accurate. As neutrons are mono-energetic, this analysis does not account for the effect on one-group cross-sections of the changing neutron spectrum with burn-up. The flux varies from $x = 0$ to $x = L$, where L is the length of the problem, subject to reflective boundary conditions:

$$\left.\frac{\partial\phi}{\partial x}\right|_{x=0}=\left.\frac{\partial\phi}{\partial x}\right|_{x=L}=0 \tag{7}$$

The Bateman equation can be written as:

$$\frac{\partial N}{\partial t}=\left(\mathbf{\Sigma}\phi+\mathbf{\Lambda}\right)N \tag{8}$$

Here N is the nuclide density vector at a point in space, t is the time variable, $\mathbf{\Sigma}$ is the matrix containing microscopic cross-sections and fission yields which correspond to all neutron-induced transmutation, and $\mathbf{\Lambda}$ is the matrix of decay constants, describing the loss and gain of nuclide densities due to decay. The nuclide density field has the initial condition:

$$N(x,0)=N_0 \tag{9}$$

The diffusion solution is evaluated at several discrete time-points, denoted by the index n, such that the diffusion solution at a given time-point is:

$$-\frac{1}{3\Sigma_{\mathrm{t},n}}\frac{\partial^2\phi_n}{\partial x^2}+\Sigma_{\mathrm{a},n}\phi_n=\frac{1}{k_n}\nu\Sigma_{\mathrm{f},n}\phi_n \tag{10}$$

The coupling from the isotopic composition to the neutronics is due to the macroscopic cross-sections, $\Sigma_{\mathrm{r},n}$ – here r signifies any of the reaction types featuring in Eq. (10). Each macroscopic cross-section can be written as:

$$\Sigma_{\mathrm{r},n}=\sigma_{\mathrm{r}}^{T}N_n \tag{11}$$

Here σ_{r} is the vector of microscopic cross-sections of reaction type r. An Euler discretisation of Eq. (8) gives:

$$N_{n+1}=[\mathbf{I}+\Delta t(\mathbf{\Sigma}\phi_n+\mathbf{\Lambda})]N_n \tag{12}$$

In the above equation, $\mathbf{I}$ is the identity matrix and Δt is the time-step length, or the time difference between t_{n+1} and t_n. This is a much simpler treatment than the matrix exponential shown in Eq. (2): the time discretisation shown here is coarse and will struggle to resolve stiff systems (such as those commonly encountered in burn-up). However, this discretisation is equivalent to Taylor expanding the matrix exponential to first order, as is necessary to make the linear stability analysis tractable – or at least to obtain analytic expressions. Nevertheless, all simulations that follow will use the matrix exponential evaluation – this does not appear to affect the accuracy of the stability analysis for the problems considered.

A stability analysis of the discretised Eqs. (10) and (12) is contained within Densmore et al. (2013). This work extends theirs by considering several other depletion schemes as well, beginning with the predictor-corrector scheme. Specifically, the above equation now only provides an intermediate 'predictor' nuclide density vector:

$$N_{n+1}^{(0)} = [\mathbf{I} + \Delta t(\mathbf{\Sigma}\phi_n + \mathbf{\Lambda})]N_n \tag{13}$$

The superscript (0) is used to emphasise that this is not the final N_{n+1} nuclide density. The corresponding intermediate flux solution, $\phi_{n+1}^{(0)}$, is obtained from the same equation as before, albeit with macroscopic cross-sections corresponding to the $N_{n+1}^{(0)}$ nuclide density field. The corrector depletion equation – yielding the nuclide density at the next time-point – is:

$$N_{n+1} = \left[\mathbf{I} + \Delta t\left(\mathbf{\Sigma}\frac{\phi_n + \phi_{n+1}^{(0)}}{2} + \mathbf{\Lambda}\right)\right] N_n \tag{14}$$

Before proceeding to the stability analysis, one should note that the stable solution produces a spatially uniform flux. This also requires a normalisation, which is usually to power in burn-up calculations. For this 1D system, the normalisation is to power per unit area, P, thus enforcing that while the problem remains uniform:

$$\phi_n = \frac{P}{\Sigma_{\mathrm{f},n} L} \tag{15}$$

Furthermore, as there is no leakage, the eigenvalue for the spatially uniform system can be asserted as:

$$k_n = \frac{\nu\Sigma_{\mathrm{f},n}}{\Sigma_{\mathrm{a},n}} \tag{16}$$

3.2. Stability analysis

Following the stability analysis applied by Densmore et al., the variables are rewritten in terms of small perturbations to their initial values:

$$N_n = N_0 + \delta N_n \tag{17}$$

$$\phi_n = \phi_0 + \delta\phi_n \tag{18}$$

$$k_n = k_0 + \delta k \tag{19}$$

These expressions are inserted into the discretised equations above, expanded, and linearised in the perturbation terms. Doing this explicitly, the diffusion equation can be written as:

$$\begin{aligned} &- \frac{1}{3(\Sigma_{\mathrm{t},0} + \delta\Sigma_{\mathrm{t},n})} \frac{\partial^2(\phi_0 + \delta\phi_n)}{\partial x^2} \\ &+ \left[\Sigma_{\mathrm{a},0} + \delta\Sigma_{\mathrm{a},n} - \frac{1}{k_0 + \delta k_n}\left(\nu\Sigma_{\mathrm{f},0} + \nu\delta\Sigma_{\mathrm{f},n}\right)\right](\phi_0 + \delta\phi_n) = 0 \end{aligned} \tag{20}$$

Expanding the denominators and neglecting second-order terms gives:

$$\begin{aligned} -\frac{1}{3\Sigma_{\mathrm{t},0}}\frac{\partial^2\phi_0}{\partial x^2} - \frac{1}{3\Sigma_{\mathrm{t},0}}\frac{\partial^2\delta\phi_n}{\partial x^2} + \frac{\delta\Sigma_{\mathrm{t},n}}{3\Sigma_{\mathrm{t},0}^2}\frac{\partial^2\phi_0}{\partial x^2} + \Sigma_{\mathrm{a},0}(\phi_0 + \delta\phi_n) + \delta\Sigma_{\mathrm{a},n}\phi_0 \\ + \frac{\delta k_n}{k_0^2}\nu\Sigma_{\mathrm{f},0}\phi_0 - \frac{1}{k_0}\left(\nu\Sigma_{\mathrm{f},0}\phi_0 + \nu\delta\Sigma_{\mathrm{f},n}\phi_0 + \nu\Sigma_{\mathrm{f},0}\delta\phi_n\right) = 0 \end{aligned} \tag{21}$$

Noting that ϕ_0 is spatially constant and the definition of k_0 as the ratio of the initial neutron production and absorption cross-sections, the above simplifies to:

$$-\frac{1}{3\Sigma_{\mathrm{t},0}}\frac{\partial^2\delta\phi_n}{\partial x^2} = \left(\frac{\delta\Sigma_{\mathrm{f},n}}{\Sigma_{\mathrm{f},0}} - \frac{\delta\Sigma_{\mathrm{a},n}}{\Sigma_{\mathrm{a},0}} - \frac{\delta k_n}{k_0}\right)\Sigma_{\mathrm{a},0}\phi_0 \tag{22}$$

Repeating the same for the nuclide density field:

$$N_0 + \delta N_{n+1}^{(0)} = \left[\mathbf{I} + \Delta t(\mathbf{\Sigma}(\phi_0 + \delta\phi_n) + \mathbf{\Lambda})\right](N_0 + \delta N_n) \tag{23}$$

The N_0 term on the left-hand side cancels with the $\mathbf{I}N_0$ term on the right-hand side. Neglecting second-order terms leaves:

$$\delta N_{n+1}^{(0)} = \left[\mathbf{I} + \Delta t(\mathbf{\Sigma}\phi_0 + \mathbf{\Lambda})\right]\delta N_n + \Delta t(\mathbf{\Sigma}\phi_0 + \mathbf{\Lambda})N_0 + \Delta t\mathbf{\Sigma}\delta\phi_n N_0 \tag{24}$$

The intermediate flux perturbation, $\delta\phi_{n+1}^{(0)}$, is obtained from an identical equation to Eq. (22), but using the predictor nuclide density field. Finally, expanding Eq. (14) in the perturbation terms, one obtains the new nuclide density vector perturbation as:

$$\begin{aligned} \delta N_{n+1} &= \left[\mathbf{I} + \Delta t\left(\mathbf{\Sigma}\phi_0 + \mathbf{\Lambda}\right)\right]\delta N_n \\ &+ \Delta t(\mathbf{\Sigma}\phi_0 + \mathbf{\Lambda})N_0 + \frac{\Delta t}{2}\mathbf{\Sigma}\left(\delta\phi_n + \delta\phi_{n+1}^{(0)}\right)N_0 \end{aligned} \tag{25}$$

From here, the classic Von Neumann stability analysis decomposes the perturbations in the fields into Fourier modes:

$$\delta\phi_n(x) = \sum_{m=0}^{\infty}\delta\phi_{n,m}\cos\left(\frac{m\pi x}{L}\right) \tag{26}$$

$$\delta N_n(x) = \sum_{m=0}^{\infty}\delta N_{n,m}\cos\left(\frac{m\pi x}{L}\right) \tag{27}$$

The orthogonality of each Fourier mode can be used to analyse their evolution separately. Using Eq. (11) to express the macroscopic cross-sections in terms of nuclide densities, the perturbed diffusion equation, Eq. (22), for the m-th mode becomes:

$$\frac{1}{3\Sigma_{\mathrm{t},0}}\delta\phi_{n,m}\left(\frac{m\pi}{L}\right)^2 = \left(\frac{\sigma_{\mathrm{f}}^T}{\Sigma_{\mathrm{f},0}}\delta N_{n,m} - \frac{\sigma_a^T}{\Sigma_{a,0}}\delta N_{n,m} - \frac{\delta k_n}{k_0}\delta_{m0}\right)\Sigma_{\mathrm{a},0}\phi_0 \tag{28}$$

As Densmore et al. highlight, the Kronecker delta term, δ_{m0}, occurs because $\frac{\delta k_n}{k_0}$ is spatially-constant, only contributing to the zeroth solution mode. When $m > 0$, Eq. (28) can be solved for the flux mode:

$$\delta\phi_{n,m} = \phi_0\left(\frac{L}{m\pi L_D}\right)^2\left(\frac{\sigma_{\mathrm{f}}^T}{\Sigma_{\mathrm{f},0}} - \frac{\sigma_{\mathrm{a}}^T}{\Sigma_{\mathrm{a},0}}\right)\delta N_{n,m} \tag{29}$$

The L_D term is the diffusion length, equal to $\frac{1}{\sqrt{3\Sigma_{\mathrm{t},0}\Sigma_{\mathrm{a},0}}}$. Inserting Eq. (29) into Eq. (24), the predictor nuclide density error vector can be expressed as:

$$\begin{aligned}\delta N_{n+1,m}^{(0)} &= \left[\mathbf{I} + \Delta t(\mathbf{\Sigma}\phi_0 + \mathbf{\Lambda})\right]\delta N_{n,m} \\ &+ \Delta t(\mathbf{\Sigma}\phi_0 + \mathbf{\Lambda})N_0\delta_{m0} + \Delta t\mathbf{\Sigma}\delta\phi_{n,m}N_0\end{aligned} \tag{30}$$

This, likewise, contains a Kronecker delta term due to spatially-constant contributions. Inserting the expression for the flux modes from Eq. (29), for $m > 0$ this becomes:

$$\begin{aligned}\delta N_{n+1,m}^{(0)} &= \left[\mathbf{I} + \Delta t(\mathbf{\Sigma}\phi_0 + \mathbf{\Lambda})\right]\delta N_{n,m} \\ &+ \Delta t\mathbf{\Sigma}N_0\phi_0\left(\frac{L}{m\pi L_D}\right)^2\left(\frac{\sigma_{\mathrm{f}}^T}{\Sigma_{\mathrm{f},0}} - \frac{\sigma_{\mathrm{a}}^T}{\Sigma_{\mathrm{a},0}}\right)\delta N_{n,m}\end{aligned} \tag{31}$$

Or, more succinctly:

$$\delta N_{n+1,m}^{(0)} = \mathbf{M}_m\delta N_{n,m} \tag{32}$$

with:

$$\mathbf{M}_m = \left[\left[\mathbf{I} + \Delta t(\mathbf{\Sigma}\phi_0 + \mathbf{\Lambda})\right] + \Delta t\mathbf{\Sigma}N_0\phi_0\left(\frac{L}{m\pi L_D}\right)^2\left(\frac{\sigma_{\mathrm{f}}^T}{\Sigma_{\mathrm{f},0}} - \frac{\sigma_{\mathrm{a}}^T}{\Sigma_{\mathrm{a},0}}\right)\right] \tag{33}$$

This expression was obtained by Densmore et al. (2013). Incidentally, numerical instability observed in Monte Carlo burn-up problems is often partly attributed to the high dominance ratio of the particular problem. Eq. (33) can be used to link this observation to theory. The dominance ratio is defined as:

$$\rho = \frac{k_1}{k_0} \tag{34}$$

In this instance, rather than denoting time-points, the subscripts denote the eigenvalues of different harmonics of the diffusion equation – k_0 is the fundamental eigenvalue, or k_{eff}. For the problem considered here, the initial dominance ratio, ρ_0, can be obtained analytically as:

$$\rho_0 = \frac{1}{1 + \left(\frac{\pi L_D}{L}\right)^2} \tag{35}$$

Therefore, for $m = 1$, Eq. (33) can be expressed in terms of ρ_0 as:

$$\mathbf{M}_1 = \left[[\mathbf{I} + \Delta t(\mathbf{\Sigma}\phi_0 + \mathbf{\Lambda})] + \Delta t \mathbf{\Sigma} N_0 \phi_0 \frac{\rho_0}{1-\rho_0} \left(\frac{\sigma_{\mathrm{f}}^T}{\Sigma_{\mathrm{f},0}} - \frac{\sigma_{\mathrm{a}}^T}{\Sigma_{\mathrm{a},0}} \right) \right] \tag{36}$$

Hence, as $\rho_0 \to 1$, the norm of the matrix (and the magnitude of its eigenvalues) will approach infinity, making the problem more unstable.

In order to conclude the analysis from Densmore et al. before extending it further, obtaining the solutions for the $m = 0$ modes should also be demonstrated. As stated above, the $m = 0$ flux mode cannot be obtained directly from Eq. (29). Instead, the power normalisation is used, and, in particular, Eq. (15) is expanded with the $m = 0$ flux and nuclide density vector modes. This gives:

$$(\phi_0 + \delta\phi_{n,0})\, \sigma_{\mathrm{f}}^T\, (N_0 + \delta N_{n,0}) = P/L \tag{37}$$

The $\phi_0 \Sigma_{\mathrm{f},0}$ term is equal to P/L. Therefore, neglecting the second-order term:

$$\delta\phi_{n,0} \Sigma_{\mathrm{f},0}^T + \sigma_{\mathrm{f}}^T \delta N_{n,0} \phi_0 = 0 \tag{38}$$

Rearranging finally gives:

$$\delta\phi_{n,0} = -\frac{\phi_0 \sigma_{\mathrm{f}}^T}{\Sigma_{\mathrm{f},0}} \delta N_{n,0} \tag{39}$$

This can be inserted into Eq. (30) to give:

$$\begin{aligned} \delta N_{n+1,0}^{(0)} &= [\mathbf{I} + \Delta t(\mathbf{\Sigma}\phi_0 + \mathbf{\Lambda})]\, \delta N_{n,0} \\ &+ \Delta t(\mathbf{\Sigma}\phi_0 + \mathbf{\Lambda}) N_0 - \Delta t \mathbf{\Sigma} N_0 \frac{\phi_0 \sigma_{\mathrm{f}}^T}{\Sigma_{\mathrm{f},0}} \delta N_{n,0} \end{aligned} \tag{40}$$

or:

$$\delta N_{n+1,0}^{(0)} = \mathbf{M}_0 \delta N_{n,0} + \Delta t(\mathbf{\Sigma}\phi_0 + \mathbf{\Lambda}) N_0 \tag{41}$$

with:

$$\mathbf{M}_0 = \left[[\mathbf{I} + \Delta t(\mathbf{\Sigma}\phi_0 + \mathbf{\Lambda})] - \Delta t \mathbf{\Sigma} N_0 \frac{\phi_0 \sigma_{\mathrm{f}}^T}{\Sigma_{\mathrm{f},0}} \right] \tag{42}$$

These results are identical to those obtained by Densmore et al., if the $N_{n+1}^{(0)}$ value is accepted as the updated nuclide density vector for the next time-step. From this point the remainder of the work presented is entirely original. Extending the analysis to the predictor-corrector scheme requires also considering the corrector update equation for the nuclide density vector. These corrector nuclide density vector modes are given by:

$$\begin{aligned} \delta N_{n+1,m} &= [\mathbf{I} + \Delta t\, (\mathbf{\Sigma}\phi_0 + \mathbf{\Lambda})] \delta N_{n,m} \\ &+ \Delta t(\mathbf{\Sigma}\phi_0 + \mathbf{\Lambda}) N_0 \delta_{m0} + \frac{\Delta t}{2} \mathbf{\Sigma} N_0 \left(\delta\phi_{n,m} + \delta\phi_{n+1,m}^{(0)} \right) \end{aligned} \tag{43}$$

Considering the $m > 0$ modes first gives:

$$\delta N_{n+1,m} = [\mathbf{I} + \Delta t\,(\mathbf{\Sigma}\phi_0 + \mathbf{\Lambda})]\delta N_{n,m} + \frac{\Delta t}{2}\mathbf{\Sigma}N_0\left(\delta\phi_{n,m} + \delta\phi^{(0)}_{n+1,m}\right) \tag{44}$$

$\delta\phi_{n,m}$ is expressed in terms of the nuclide density from Eq. (29). The nuclide density expression of $\delta\phi^{(0)}_{n+1,m}$ can be obtained straightforwardly given Eqs. (29) and (31):

$$\delta\phi^{(0)}_{n+1,m} = \Phi^T_m\left[\mathbf{B} + \Delta t\mathbf{\Sigma}N_0\Phi^T_m\right]\delta N_{n,m} \tag{45}$$

where, for brevity, two new operators are defined:

$$\Phi^T_m = \phi_0\left(\frac{L}{m\pi L_D}\right)^2\left(\frac{\sigma^T_f}{\Sigma_{\mathrm{f},0}} - \frac{\sigma^T_{\mathrm{a}}}{\Sigma_{\mathrm{a},0}}\right) \tag{46}$$

and

$$\mathbf{B} = [\mathbf{I} + \Delta t(\mathbf{\Sigma}\phi_0 + \mathbf{\Lambda})] \tag{47}$$

Hence, Eq. (44) becomes

$$\delta N_{n+1,m} = \mathbf{M}_m\delta N_{n,m} \tag{48}$$

with:

$$\mathbf{M}_m = \left[\mathbf{B} + \frac{\Delta t}{2}\mathbf{\Sigma}N_0\Phi^T_m\left[\mathbf{I} + \mathbf{B} + \Delta t\mathbf{\Sigma}N_0\Phi^T_m\right]\right] \tag{49}$$

The corresponding equation for the explicit Euler scheme, using the same notation, is:

$$\mathbf{M}_m = \left[\mathbf{B} + \Delta t\mathbf{\Sigma}N_0\Phi^T_m\right] \tag{50}$$

Noting the definition of $\mathbf{B}$, it can be seen that, in the limit of a short time-step where Δt^2 terms can be neglected, the matrix describing the evolution of the predictor-corrector Fourier modes approaches that of the explicit Euler scheme.

For the $m = 0$ mode, Eq. (43) gives:

$$\begin{aligned}\delta N_{n+1,0} &= [\mathbf{I} + \Delta t\,(\mathbf{\Sigma}\phi_0 + \mathbf{\Lambda})]\delta N_{n,0} \\ &+ \Delta t(\mathbf{\Sigma}\phi_0 + \mathbf{\Lambda})N_0 + \frac{\Delta t}{2}\mathbf{\Sigma}N_0\left(\delta\phi_{n,0} + \delta\phi^{(0)}_{n+1,0}\right)\end{aligned} \tag{51}$$

The expression for $\delta\phi^{(0)}_{n+1,0}$ in terms of $\delta N_{n,0}$ combines Eqs. (39) and (40) to give:

$$\delta\phi^{(0)}_{n+1,0} = \Phi^T_0\left[\mathbf{B} + \Delta t\mathbf{\Sigma}N_0{\Phi^T}_0\right]\delta N_{n,0} + \Phi^T_0\left[\mathbf{B} - \mathbf{I}\right]N_0 \tag{52}$$

Again for brevity:

$$\Phi^T_0 = -\frac{\phi_0\sigma^T_{\mathrm{f}}}{\Sigma_{\mathrm{f},0}} \tag{53}$$

With this, Eq. (51) can be written:

$$\delta N_{n+1,0} = \mathbf{M}_0 \delta N_{n,0} + \mathbf{K}_0 N_0 \tag{54}$$

with:

$$\mathbf{M}_0 = \left[\mathbf{B} + \frac{\Delta t}{2} \mathbf{\Sigma} N_0 \Phi_0^T \left[\mathbf{I} + \mathbf{B} + \Delta t \mathbf{\Sigma} N_0 \Phi_0^T \right] \right] \tag{55}$$

and:

$$\mathbf{K}_0 = \left[\mathbf{I} + \frac{\Delta t}{2} \mathbf{\Sigma} N_0 \Phi_0^T \right] \left[\mathbf{B} - \mathbf{I} \right] \tag{56}$$

On the other hand, the explicit Euler expressions are:

$$\mathbf{M}_0 = \left[\mathbf{B} + \Delta t \mathbf{\Sigma} N_0 \Phi_0^T \right] \tag{57}$$

and:

$$\mathbf{K}_0 = \left[\mathbf{B} - \mathbf{I} \right] \tag{58}$$

Again the predictor-corrector equations reduce to their explicit Euler counterparts in the limit of short Δt: this comes from inserting the definition of $\mathbf{B}$ into Eqs. (55) and (56) and neglecting Δt^2 terms.

3.3. Multiple corrector iterations

This analysis can be extended further to performing more than one corrector iteration. Consider adding a second corrector step – the previous 'corrector' $n+1$ values are now also denoted with a superscript (1). Performing a second corrector iteration, the $(n+1)$-th nuclide density is obtained from:

$$N_{n+1}^{(2)} = \left[\mathbf{I} + \Delta t \left(\mathbf{\Sigma} \frac{\phi_n + \phi_{n+1}^{(1)}}{2} + \mathbf{\Lambda} \right) \right] N_n \tag{59}$$

The flux solution after the first corrector step, $\phi_{n+1}^{(1)}$, is obtained from the corresponding nuclide density vector as before, with the same operator relating the nuclide density modes to the flux modes, Φ_m^T or Φ_0^T. Furthermore, the expression for $\delta N_{n+1,m}^{(1)}$ is simply one of Eqs. (48) or (54). For the former ($m > 0$) case, one obtains:

$$\delta N_{n+1,m}^{(2)} = \left[\mathbf{B} + \frac{\Delta t}{2} \mathbf{\Sigma} N_0 \Phi_m^T \left[\mathbf{I} + \mathbf{M}_m^{(1)} \right] \right] \delta N_{n,m} \tag{60}$$

where $\mathbf{M}_m^{(1)}$ is given by Eq. (49). This can be used to initialise a recurrence relation for J corrector iterations, giving:

$$\delta N_{n+1,m}^{(J)} = \mathbf{M}_m^{(J)} \delta N_{n,m} \tag{61}$$

and:

$$\mathbf{M}_m^{(J)} = \left[\mathbf{B} + \frac{\Delta t}{2} \mathbf{\Sigma} N_0 \Phi_m^T \left[\mathbf{I} + \mathbf{M}_m^{(J-1)} \right] \right] \tag{62}$$

The same logic applies to obtaining the expression for the $m = 0$ mode subject to multiple corrector iterations. Making use of the expressions in Eqs. (55) and (56), one obtains:

$$\begin{aligned}\delta N^{(2)}_{n+1,0} = &\left[\mathbf{B} + \frac{\Delta t}{2}\mathbf{\Sigma} N_0 \Phi_0^T \left[\mathbf{I} + \mathbf{M}_0\right]\right] \delta N_{n,0} \\ &+ \left[\mathbf{B} - \mathbf{I} + \frac{\Delta t}{2}\mathbf{\Sigma} N_0 \Phi_0^T \mathbf{K}_0\right] N_0\end{aligned} \tag{63}$$

Once again, for J corrector iterations, this is convenient to write as a recurrence relation, initialised by Eqs. (55) and (56), such that one has:

$$\delta N^{(J)}_{n+1,0} = \mathbf{M}_0^{(J)} \delta N_{n,0} + \mathbf{K}_0^{(J)} N_0 \tag{64}$$

where:

$$\mathbf{M}_0^{(J)} = \left[\mathbf{B} + \frac{\Delta t}{2}\mathbf{\Sigma} N_0 \Phi_0^T \left[\mathbf{I} + \mathbf{M}_0^{(J-1)}\right]\right] \tag{65}$$

and:

$$\mathbf{K}_0^{(J)} = \left[\mathbf{B} - \mathbf{I} + \frac{\Delta t}{2}\mathbf{\Sigma} N_0 \Phi_0^T \mathbf{K}_0^{(J-1)}\right] \tag{66}$$

3.4. Relaxation on the corrector iteration

Finally, one might ask how relaxation affects the stability of the corrector iteration. In particular, the corrector equation is modified such that performing J corrector iterations is expressed as:

$$N^{(J)}_{n+1} = \alpha \left[\mathbf{I} + \Delta t \left(\mathbf{\Sigma}\frac{\phi_n + \phi^{(J-1)}_{n+1}}{2} + \mathbf{\Lambda}\right)\right] N_n + (1-\alpha) N^{(J-1)}_{n+1} \tag{67}$$

Here, α is a relaxation factor, taking a value between 0 and 1. Beginning, as in the previous section, with a single corrector iteration, one has:

$$N^{(1)}_{n+1} = \alpha \left[\mathbf{I} + \Delta t \left(\mathbf{\Sigma}\frac{\phi_n + \phi^{(0)}_{n+1}}{2} + \mathbf{\Lambda}\right)\right] N_n + (1-\alpha) N^{(0)}_{n+1} \tag{68}$$

Following the same steps as before, for $m > 0$ and a single corrector iteration, one ultimately obtains:

$$\delta N^{(1)}_{n+1,m} = \tilde{\mathbf{M}}_m \delta N_{n,m} \tag{69}$$

with

$$\begin{aligned}\tilde{\mathbf{M}}_m = &\alpha \left(\mathbf{B} + \frac{\Delta t}{2}\mathbf{\Sigma} N_0 \Phi_m^T \left[\mathbf{I} + \mathbf{B} + \Delta t \mathbf{\Sigma} N_0 \Phi_m^T\right]\right) \\ &+ (1-\alpha)\left(\mathbf{B} + \Delta t \mathbf{\Sigma} N_0 \Phi_m^T\right)\end{aligned} \tag{70}$$

The most convenient way to write this for multiple corrector iterations is to use the matrix $\tilde{\mathbf{M}}_m$ in a recurrence relation, such that, for $J > 1$ corrector iterations, one has:

$$\delta N_{n+1,m}^{(J)} = \tilde{\mathbf{M}}_m^{(J)} \delta N_{n,m} \tag{71}$$

where

$$\tilde{\mathbf{M}}_m^{(J)} = \left[\alpha \left[\mathbf{B} + \frac{\Delta t}{2}\mathbf{\Sigma} N_0 \Phi_m^T\right] + \left[(1-\alpha)\mathbf{I} + \alpha\frac{\Delta t}{2}\mathbf{\Sigma} N_0 \Phi_m^T\right] \tilde{\mathbf{M}}_m^{(J-1)}\right] \tag{72}$$

with $\tilde{\mathbf{M}}_m^{(1)}$ given by Eq. (70).

From expanding Eq. (68), the $m = 0$ mode is given by:

$$\begin{aligned}\delta N_{n+1,0}^{(1)} = \alpha &\left[\mathbf{B} + \frac{\Delta t}{2}\mathbf{\Sigma} N_0 \Phi_0^T\right] \delta N_{n,0} \\ &+ \left[(1-\alpha)\mathbf{I} + \alpha\frac{\Delta t}{2}\mathbf{\Sigma} N_0 \Phi_0^T\right] \delta N_{n+1,0}^{(0)} \\ &+ [\mathbf{B} - \mathbf{I}]\, N_0\end{aligned} \tag{73}$$

The expression for $\delta N_{n+1,0}^{(0)}$ is the same as before from Eq. (40), giving an expression for the first corrector iteration as:

$$\delta N_{n+1,0}^{(1)} = \tilde{\mathbf{M}}_0 \delta N_{n,0} + \tilde{\mathbf{K}}_0 N_0 \tag{74}$$

where

$$\tilde{\mathbf{M}}_0 = \left[\mathbf{B} + (1-\alpha)\Delta t \mathbf{\Sigma} N_0 \Phi_0^T + \alpha\frac{\Delta t}{2}\mathbf{\Sigma} N_0 \Phi_0^T \left[\mathbf{I} + \mathbf{B} + \Delta t \mathbf{\Sigma} N_0 \Phi_0^T\right]\right] \tag{75}$$

$$\tilde{\mathbf{K}}_0 = \left[(2-\alpha)\mathbf{I} + \alpha\frac{\Delta t}{2}\mathbf{\Sigma} N_0 \Phi_0^T\right] [\mathbf{B} - \mathbf{I}] \tag{76}$$

Extending this to J iterations results in a similar expression as for the $m > 0$ modes, with:

$$\delta N_{n+1,0}^{(J)} = \tilde{\mathbf{M}}_0^{(J)} \delta N_{n,0} + \tilde{\mathbf{K}}_0^{(J)} N_0 \tag{77}$$

with the recurrence relations for each operator as:

$$\tilde{\mathbf{M}}_0^{(J)} = \left[\alpha \left[\mathbf{B} + \frac{\Delta t}{2}\mathbf{\Sigma} N_0 \Phi_0^T\right] + \left[(1-\alpha)\mathbf{I} + \alpha\frac{\Delta t}{2}\mathbf{\Sigma} N_0 \Phi_0^T\right] \tilde{\mathbf{M}}_0^{(J-1)}\right] \tag{78}$$

and:

$$\tilde{\mathbf{K}}_0^{(J)} = \left[\mathbf{B} - \mathbf{I} + \left[(1-\alpha)\mathbf{I} + \alpha\frac{\Delta t}{2}\mathbf{\Sigma} N_0 \Phi_0^T\right] \tilde{\mathbf{K}}_0^{(J-1)}\right] \tag{79}$$

The $\tilde{\mathbf{M}}_0^{(1)}$ and $\tilde{\mathbf{K}}_0^{(1)}$ terms are given by Eqs. (75) and (76), respectively. For each of these expressions for the matrices governing the growth of the Fourier modes, the analysis can be applied to the stochastic approximation in particular by letting α vary with each iteration as $\frac{1}{j+1}$ where j is the iteration number.

4. Numerical investigations

With the matrices obtained from the previous section one can examine how their predictions agree with simulation. This will be done using the simple two-nuclide system given by Densmore et al. (2013). In this system only two nuclides are present: one fissile, one fission product, both without decay. Their microscopic cross-sections (in barns) are:

$$\sigma_{\mathrm{t}} = \begin{bmatrix} 4000 \\ 150 \end{bmatrix} \quad \sigma_{\mathrm{a}} = \begin{bmatrix} 3000 \\ 150 \end{bmatrix} \quad \sigma_{\mathrm{f}} = \begin{bmatrix} 3000 \\ 0 \end{bmatrix}$$

With a fission yield of the fission product of 1, this gives $\mathbf{\Sigma}$ as:

$$\mathbf{\Sigma} = \begin{bmatrix} -3000 & 0 \\ 3000 & -150 \end{bmatrix}$$

The initial nuclide density in (atoms/b/cm) is:

$$N_0 = \begin{bmatrix} 0.00025 \\ 0 \end{bmatrix}$$

The average neutron production, ν, is 2.3, the power per unit area is 10 kW/cm^2, and fission produces 200 MeV of energy. The geometry is 3 m long.

As the system and its eigenvalues are quite simple, the eigenvalues corresponding to one particular eigenvector will be shown, rather than the spectral radius. The other set of eigenvectors for all spatial modes have a constant eigenvalue of 1 for all time-step lengths and so do not determine stability.

For the predictor-corrector scheme, the eigenvalues calculated from Eq. (49) are shown in Fig. 1. Similarly to the explicit Euler scheme as reported by Densmore et al. (2013), the first spatial mode is the most unstable. However, all eigenvalues are positive here rather than negative – this implies that instability with the predictor-corrector scheme manifests not as an oscillation to begin, but as a growing asymmetry. This behaviour has been previously reported for high-fidelity neutronics and depletion problems using the predictor-corrector scheme (Isotalo, 2013; Cosgrove et al., 2020a). Simulating the results for various time-step lengths appears to support the eigenvalue predictions – this is shown in Fig. 2. It can be seen that below the critical time-step of about 5.5 days no higher spatial modes are excited. Above this, however, the first spatial mode begins to amplify without oscillation – as only the first spatial mode has a positive eigenvalue with magnitude greater than one for this time-step length, this corresponds well with Fig. 1.

Varying the number of corrector iterations from 0 (or the explicit Euler scheme) to 5, the eigenvalues of the first spatial mode (which is the most unstable in all cases) are plotted in Fig. 3. These are obtained from Eqs. (49) and (62). This shows, as reported by Cosgrove et al. (2020a), that the nature of the instability – whether it is an oscillation or an amplifying asymmetry – will depend upon the number of corrector iterations performed. Intriguingly, for this problem, the maximum stable time-step length is identical for all coupling schemes – this is due to the simplicity of the particular depletion system and is not generally the case. In

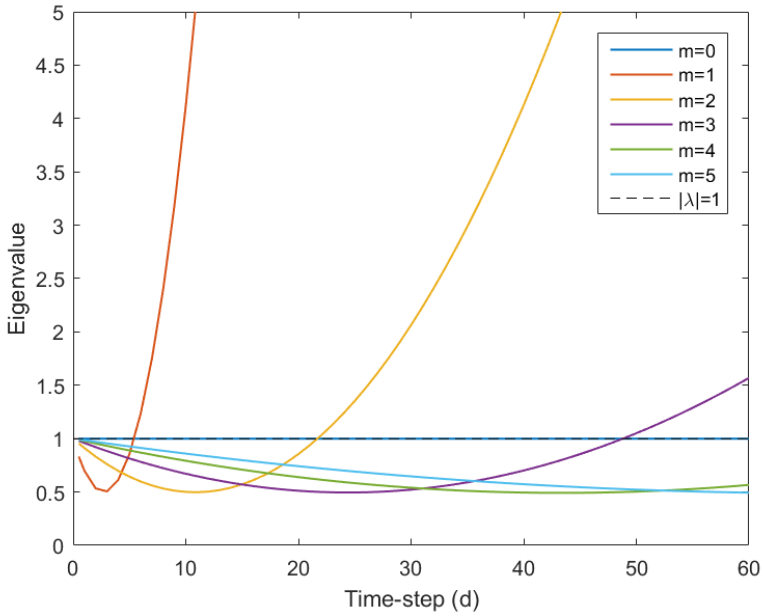

Fig. 1. Eigenvalues of the predictor-corrector scheme with time-step.

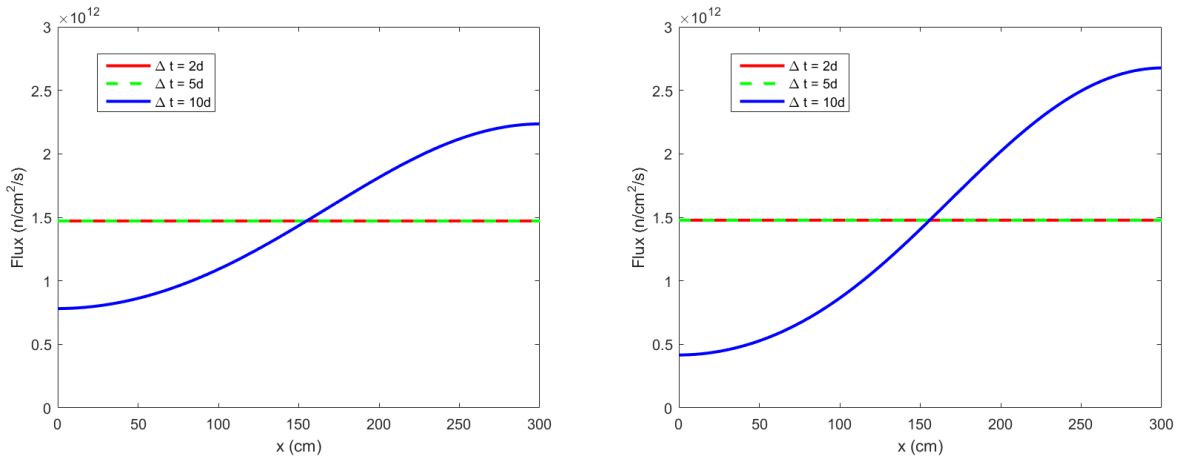

(a) 160 days **(b)** 170 days

Fig. 2. Predictor-corrector flux solutions at consecutive time-points.

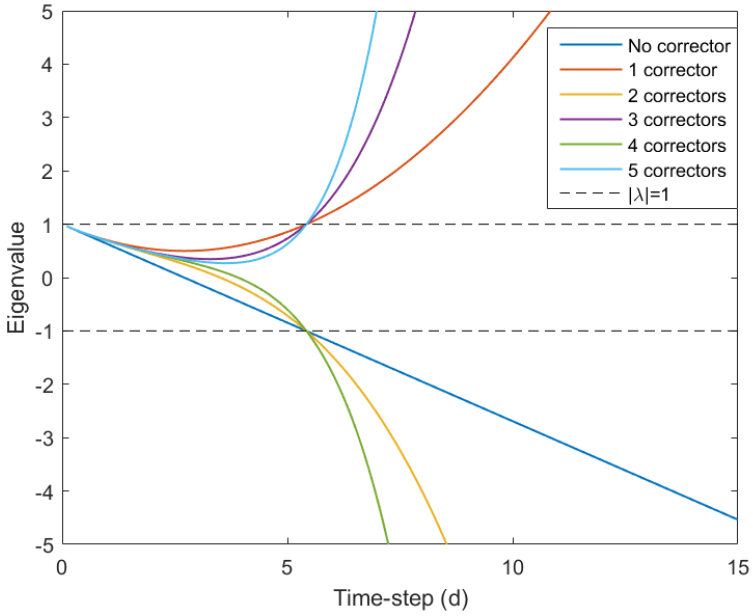

Fig. 3. Eigenvalues of the first spatial mode with time-step when varying the number of corrector iterations.

fact, the stable time-steps for higher spatial modes are noticeably non-coincident. That being said, above the maximum stable time-step the magnitude of the unstable eigenvalue grows with additional corrector iterations, implying that, while all of the schemes are unstable in this region, erroneous solution modes will grow more quickly with additional corrector steps. This was suspected to be the case and briefly discussed in Cosgrove et al. (2020a) for a reasonably representative reactor physics depletion system.

Eq. (72) is used to plot the eigenvalues of the first spatial mode when applying a relaxation over multiple iterations. Fig. 4 shows the results when using a relaxation factor of 0.1 and 0.5 alongside each other. In both cases, it can be seen that a well-chosen relaxation factor applied over several iterations will increase the maximum stable time-step length. However, too heavy a relaxation with too few iterations lends too much weight to the explicit Euler predictor, providing only marginal benefit to stability and possibly producing oscillatory instability behaviour, uncharacteristic of the predictor-corrector scheme with only a single corrector. On the other hand, too light a relaxation – even with many iterations – will give a more modest increase in the maximum stable time-step length.

Although the first spatial mode eigenvalues for various numbers of corrector iterations are shown in Fig. 4, while they tend to be dominant, this is not always the case when relaxation is applied. This is demonstrated by showing several spatial mode eigenvalues alongside flux solutions produced by a relaxed simulation taking time-steps of 50 days. Fig. 5(a) shows that when a relaxation factor of 0.1 is applied using 50 day time-steps, it is actually only the second spatial mode which is unstable. This mode is symmetric and oscillatory here, and its growth becomes apparent in the simulation shown in Fig. 5(b). This circumstance was only

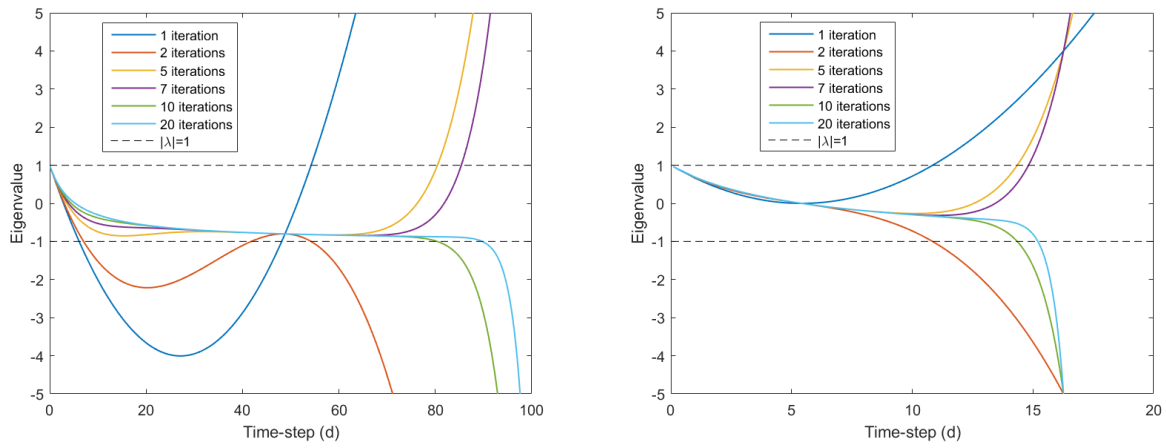

(a) $\alpha = 0.1$ **(b)** $\alpha = 0.5$

Fig. 4. Eigenvalues of the first instability mode of the predictor-corrector scheme with time-step when using multiple corrector iterations and two different relaxation factors.

devised by examining the eigenvalues: the range of time-steps for which this would have been possible is small and unlikely to be found accidentally. However, this demonstrates the possibility of symmetric instabilities (at least when applying relaxation), and so researchers undertaking future stability studies relying on symmetry as a proxy for stability should be wary.

A final investigation that this analysis permits is a comparison of different implicit schedules, similar to the examination performed in Cosgrove et al. (2020a). Fig. 6 shows the most unstable eigenvalues of the predictor-corrector scheme using 1, 5, and 10 iterations, and relaxation factors of 0.3, 0.5, and following the stochastic approximation. In all cases shown here the most unstable spatial mode was the first. The figure shows the relative effectiveness of the different relaxation schedules: using relatively few corrector iterations, a reasonably aggressive relaxation is the most effective choice for increasing the stable time-step length. However, the stability imparted by a fixed relaxation factor tends to plateau, as opposed to the stochastic approximation which is effectively unconditionally stable if infinite corrector iterations are used. That being said, in practice, one would tend to favour using fewer iterations to minimise computational expense and, for a given budget of corrector iterations, a more effective fixed relaxation factor can be chosen to maximise the time-step length.

Although only two nuclides were used here, similar results can be obtained with multiple absorbing fission products which do not decay. The results can be made identical to these presented here by appropriate scaling of the fission yields or capture cross-sections – increasing fission yields or cross-sections generally has the same effect on stability as increasing the time-step length. Likewise, including decay does not necessarily affect the stability properties substantially. However, many nuclides in realistic systems have quite short half-lives, making realistic burn-up matrices numerically stiff. Such stiff systems are not dealt with presently as they require using more complicated Bateman operators in the analysis which do not lend themselves to analytic results. Nevertheless, this is an important development

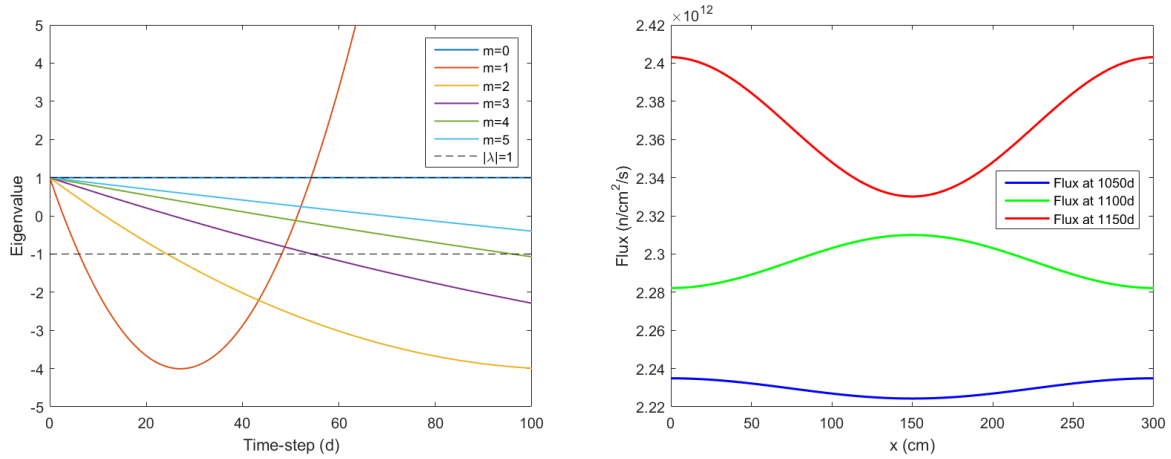

(a) Eigenvalues with time-step

(b) Fluxes at subsequent time-points

Fig. 5. Excitation of a symmetric burn-up instability using a single corrector iteration and a relaxation factor of 0.1 with a time-step of 50 days

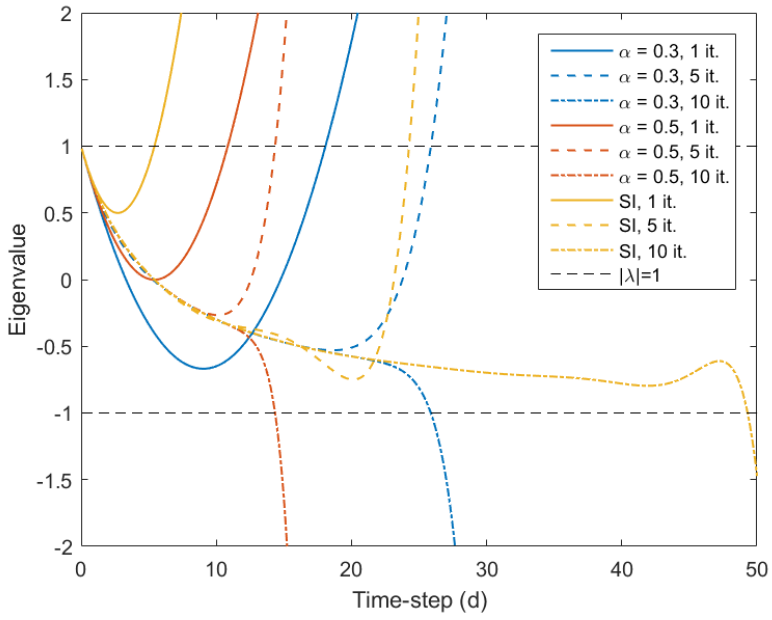

Fig. 6. Most unstable eigenvalues of several implicit predictor-corrector schemes with time-step, varying the relaxation schedule and number of iterations.

to be included in future work.

5. Conclusions

This paper has extended the previous analysis of Densmore et al. (2013) to several versions of the predictor-corrector scheme. The analysis predicts a number of results which had been previously observed in coupled neutronics-depletion calculations but left unexplained. The analysis is shown to be predictive against the simple example system used here. This includes showing that the first spatial mode tends to be the most unstable, predicting whether or not the instability behaviour is oscillatory, and demonstrating that relaxing the corrector step depresses non-physical spatial modes.

Realistic neutronics-depletion systems are substantially more complicated than those presented here, although the analysis is a first step towards considering further complexities. Importantly, realistic depletion systems are more numerically stiff than those examined here – for such systems the Euler-discretised Bateman equation is inadequate for estimating numerical stability. Hence, future work will extend the analysis to more sophisticated Bateman operators, e.g., the matrix exponential. There are also higher-order coupling schemes to consider, such as Isotalo's substep methods (Isotalo and Aarnio, 2011a,b). Furthermore, in realistic systems the one-group cross-sections and average neutron production will evolve with burn-up due to the changing spectrum – this effect should not be neglected. Additionally, the spatial discretisation of burnable regions in Monte Carlo depletion calculations is often coarse, e.g., 10 burnable regions across a fuel pin – this may have a non-negligible effect on stability which should be explored. If considering deterministic problems in future, the discretisation of the neutronic system will also be important – this is as distinct from Monte Carlo, which should be accurately described by the continuous governing neutronics equation. Hence further analysis may also account for this discretisation as well.

6. Data availability statement

To the best of the authors' knowledge, this paper and references herein contain all the data needed to reproduce and validate the results presented.

Acknowledgements

This work was carried out with the financial support of the UK Engineering and Physical Sciences Research Council (EPSRC) through the Imperial College, University of Cambridge and Open University Centre for Doctoral Training in Nuclear Energy under grant EP/L015900/1.

The authors would also like to acknowledge productive discussions held with members of the Bettis Atomic Power Laboratory and Nickolas Adamowicz of the University of Michigan.

Declarations

Declarations of interest: none.

References

Bell, G., Glasstone, S., 1970. Nuclear Reactor Theory. US Atomic Energy Commission, Washington, DC.

Cosgrove, P., Shwageraus, E., Parks, G., 2020a. A simple implicit coupling scheme for Monte Carlo neutronics and isotopic depletion. Annals of Nuclear Energy 141. doi:10.1016/j.anucene.2020.107374.

Cosgrove, P., Shwageraus, E., Parks, G.T., 2020b. Neutron clustering as a driver of Monte Carlo burn-up instability. Annals of Nuclear Energy 137. doi:10.1016/j.anucene.2019.106991.

Densmore, J.D., Gill, D.F., Griesheimer, D.P., 2013. Stability analysis of burnup calculations. Transactions of the American Nuclear Society 109, 695–698. doi:10.1007/s10967-012-2210-3.2.

Dufek, J., Kotlyar, D., Shwageraus, E., 2013. The stochastic implicit Euler method: A stable coupling scheme for Monte Carlo burnup calculations. Annals of Nuclear Energy 60, 295–300. doi:10.1016/j.anucene.2013.05.015.

Griesheimer, D.P., 2010. In-line xenon convergence algorithm for Monte Carlo reactor calculations, in: Proc. PHYSOR 2010, Pittsburgh, Pennsylvania.

Isotalo, A., 2013. Computational Methods for Burnup Calculations with Monte Carlo Neutronics. Ph.D. thesis. Aalto University.

Isotalo, A., Aarnio, P., 2011a. Higher order methods for burnup calculations with Bateman solutions. Annals of Nuclear Energy 38, 1987–1995. doi:10.1016/j.anucene.2011.04.022.

Isotalo, A., Aarnio, P., 2011b. Substep methods for burnup calculations with Bateman solutions. Annals of Nuclear Energy 38, 2509–2514. doi:10.1016/j.anucene.2011.07.012.

Isotalo, A., Sahlberg, V., 2015. Comparison of Neutronics-Depletion Coupling Schemes for Burnup Calculations. Nuclear Science and Engineering 179, 434–459. doi:10.13182/NSE14-35.

Isotalo, A.E., Leppänen, J., Dufek, J., 2013. Preventing xenon oscillations in Monte Carlo burnup calculations by enforcing equilibrium xenon distribution. Annals of Nuclear Energy 60, 78–85. doi:10.1016/j.anucene.2013.04.031.

Josey, C., 2017. Development and Analysis of High Order Neutron Transport-Depletion Coupling Algorithms. Ph.D. thesis. Massachusetts Institute of Technology.

Kotlyar, D., Shwageraus, E., 2014. Numerically stable Monte Carlo-burnup-thermal hydraulic coupling schemes. Annals of Nuclear Energy 63, 371–381. doi:10.1016/j.anucene.2013.08.016.

Kotlyar, D., Shwageraus, E., 2016. Stochastic semi-implicit substep method for coupled depletion Monte-Carlo codes. Annals of Nuclear Energy 92, 52–60. doi:10.1016/j.anucene.2016.01.022.

Pusa, M., 2013. Numerical Methods for Nuclear Fuel Burnup Calculations. Ph.D. thesis. VTT Technical Research Centre of Finland.

Robbins, H., Monro, S., 1951. A Stochastic Approximation Method. The Annals of Mathematical Statistics 22, 400–407. doi:10.1214/aoms/1177729586.

Valtavirta, V., Leppänen, J., 2018. New stochastic substep based burnup scheme for Serpent 2, in: Proc. PHYSOR 2018, Cancún, Mexico.